Edinburgh Research Explorer

Photocatalytic treatment of saccharin and bisphenol-A in the presence of TiO2 nanocomposites tuned by Sn(IV)

1   **Photocatalytic treatment of saccharin and bisphenol-A in the presence of TiO$_2$ nanocomposites tuned by**

2   **Sn(IV)**

3   **K. Davididou[1], E. Hale[1], N. Lane[1], E. Chatzisymeon[1*], A. Pichavant[2,3], J.-F. Hochepied[2,3]**

4

5   (1) Institute for Infrastructure and Environment, School of Engineering, The University of Edinburgh, Edinburgh

6   EH9 3JL, United Kingdom.

7   (2) MINES ParisTech, PSL Research University, Centre des Matériaux, BP87 91003 Evry, France.

8   (3) ENSTA ParisTech, Unité Chimie et Procédés, 828 Bd des Maréchaux, 91762 Palaiseau Cedex, France.

9

10

11   *Corresponding author: E-mail: e.chatzisymeon@ed.ac.uk; Tel.: +44 1316505711

12 **Abstract**

13 This study deals with the photocatalytic treatment of saccharin (SAC) and bisphenol-A (BPA) under UV irradiation.

14 For this purpose, novel submicronic anatase–rutile nanocomposite particles with tuned phase ratio produced by

15 thermohydrolysis of acidic Ti(IV) solutions in the presence of controlled amounts of Sn(IV) were used. These

16 catalysts were then assessed regarding their efficiency to degrade SAC or BPA, which are contaminants of

17 increased environmental and health concern. The effect of various operating conditions, such as the anatase-rutile

18 ratio (100:0, 85:15, 70:30), catalyst concentration (50-600 mg/L) and solute concentration (3-10 mg/L) was

19 investigated. Furthermore, catalyst reuse -an important but little studied aspect- was assessed. Anatase–rutile

20 nanocomposites were successfully prepared presenting good crystallinity and surface quality. Their activity was

21 about the same for removing SAC or BPA from water. It was found that photocatalytic performance was increased

22 with catalyst loading up to 400 mg/L. A further increase to 600 mg/L did not significantly enhance BPA removal,

23 thus associating this tendency with screening effects. Also, photocatalytic efficiency was increased with initial

24 solute concentration decrease. Organics degradation followed a pseudo-first order kinetic rate in terms of both

25 SAC and BPA removal. The reproducibility of catalyst activity was assessed in three successive reuse cycles,

26 where the removal percentage of initially 5 mg/L SAC was maintained as high as 70% at the end of the 3rd cycle,

27 in the presence of initially 400 mg/L anatase catalyst, and after 90 min of treatment. Finally, additional experimental

28 runs were carried out with ultrasound cleaning (US) being applied to the reactant mixture at the beginning of each

29 reuse cycle, but it was found to have no significant effect on treatment efficiency.

30

31

32

1 Introduction

Endocrine disrupting compounds (EDCs) are chemicals with documented estrogenic or androgenic activity, at trace-level concentrations, that pose serious threats to human health and wildlife [1, 2]. Various chemicals have been identified as potential EDCs including pharmaceuticals, personal care products, pesticides and herbicides, industrial chemicals, heavy metals and recently artificial sweeteners (ASs) [3-5]. ASs are metabolically inert sugar substitutes, being used increasingly in food, beverages and pharmaceuticals [6, 7], which eventually end up in domestic sewage treatment plants (STPs) mainly unchanged [8, 9]. Among them, saccharin (SAC), the forerunner of ASs, has been identified in STP effluents, rivers, and groundwater aquifers [8-10], thus reflecting the inefficiency of conventional wastewater treatment processes in eliminating recalcitrant organic compounds [3, 11]. Another critical issue related to ASs is the elevation of toxicity and the production of by-products more persistent than the parent compounds during their natural attenuation [3, 12, 13]. Furthermore, bisphenol-A (BPA) is also included among the widely detectable organic xenobiotics in urban wastewaters and treated effluents [5]. BPA is used extensively in the production of polycarbonate polymers and epoxy resins and its occurrence in waterways is an emerging environmental issue since its endocrine disruption has been well documented [14]. The major routes of EDCs in the aquatic environment are via municipal and industrial STP effluent discharges [4, 5, 15]. Therefore, the current focus is on the identification of new efficient methods able to mineralise persistent organic compounds, such as SAC and BPA, and hence preventing their discharge into the environment.

Heterogeneous photocatalysis is an advanced oxidation process (AOP) that has received considerable attention in this direction as its efficiency to eliminate persistent organic compounds has been well proved [16, 17]. Photocatalytic oxidation is initiated upon UV illumination of a semiconductor catalyst, for example TiO_2 [14, 16]. Highly reactive species, mainly hydroxyl radicals (•OH), are then formed, which can attack organic pollutants until their final mineralisation into CO_2 and inorganic anions [16, 18]. Anatase TiO_2 is a widely used photocatalyst, due to its low cost and good performance, for many applications [18]. A way to enhance its photocatalytic activity is to improve the charge separation and migration to the catalyst surface by means of interfaces with semiconductor or metallic particles. In addition to material modification, the control of nano-architecture and morphology is another way to enhance catalyst performance [19]. Therefore, a combination of these two levers (i.e. creating interfaces between anatase and rutile polymorphs) could be a key asset to improve photocatalytic performance. In general,

62   homogeneous precipitation by thermohydrolysis of acidic Ti(IV) precursors is an easy way to produce titania

63   nanoparticles, yet the control of anatase–rutile ratio is rather difficult to master and is very sensitive to

64   physicochemical conditions [19]. To get anatase–rutile interfaces, co-precipitating anatase and rutile in one pot by

65   thermohydrolysis can, therefore, be a challenging task, especially if one wants to tune anatase:rutile ratio with

66   small and controlled amounts of metals that act as rutile phase promoters. In this work a direct approach, just by

67   hydrolysing as-received commercial products without additives nor surfactants, is proposed in order to produce

68   interfaced anatase-rutile photocatalysts tuned by Sn(IV).

69   It should be highlighted that the photocatalytic treatment of ASs, such as saccharin, acesulfame and sucralose,

70   has only recently started to be studied [3, 12, 13, 20]. To the best of our knowledge, only Chen et al. (2014) deal

71   with the photocatalytic degradation of SAC [21]. Specifically, they observed 93% TOC removal in the presence of

72   0.8 g/L Degussa P25, after 3 hr irradiation under a 500 W mercury lamp. Also, they found that the reaction followed

73   pseudo-first-order degradation. However, the investigation of the optimal operating parameters of a UV/TiO$_2$

74   system as described in this paper still remains a missing element in literature.

75   The overall aim of this work was to investigate the photocatalytic degradation of SAC and BPA, as contaminants

76   of emerging environmental and health concern, in the presence of novel interfaced anatase-rutile catalysts

77   produced by thermohydrolysis and tuned by Sn(IV). These catalysts showed promising photocatalytic activity for

78   phenol removal [19] and for this reason they were also employed for SAC and BPA treatment. In view of this, the

79   effect of key operating parameters, such as initial solute concentration, catalyst type, catalyst concentration and

80   reuse, on photocatalytic performance was assessed. Finally, the effect of ultrasound cleaning on catalytic activity

81   was evaluated.

82

83   **2   Materials and methods**

84   *2.1   Chemicals*

85   All chemicals used in this study were of analytical grade and without further modification. SAC (CAS No: 81-07-2)

86   and BPA (CAS No: 80-05-7) were purchased from Acros and Sigma-Aldrich, respectively. TiOSO$_4$.xH$_2$O (CAS

87   13825-74-6), SnCl$_4$.5H$_2$O (CAS 10026-06-9) and H$_2$SO$_4$ (CAS 7664-93-9) were supplied by Sigma-Aldrich.

88 Aeroxide TiO$_2$ P25 (P25) obtained from Evonik Industries, KRONOClean 7050 (KR7050) from KRONOS

89 Worldwide, Inc. and CristalACTiV PC105 (PC105) from CRISTAL were also used.

90

91 *2.2 Catalyst preparation*

92 Syntheses of anatase-rutile composites were performed according to previously published protocol [19], where low

93 quantities of Sn(IV) were used as rutile phase promoter. Pichavant et al. (2014) [19] found that rutile phase ranging

94 between X$_R$=0.15-0.3 led to the highest photocatalytic removal of phenol. Given this, R30 was the highest rutile

95 fraction to be used in the present work. In detail, TiOSO$_4$.xH$_2$O and SnCl$_4$.5H$_2$O were dissolved in distilled water

96 acidified with H$_2$SO$_4$ so that the total concentration [Ti(IV)]+[Sn(IV)] was 1.5 mol/L and the total sulphate

97 concentration was 2 mol/L. The quantity of Sn introduced, X$_{Sn}$=[Sn(IV)]/([Ti(IV)]+[Sn(IV)]), was 0, 1.7x10^{-3} and

98 6.8x10^{-3} mol/L, for pure anatase (ANA), 15% rutile (R15) and 30% rutile (R30) catalyst samples, respectively. The

99 obtained transparent solutions were transferred into Teflon vials and heated in a microwave oven (Synthos 3000,

100 Anton Paar), without stirring, following a ramp from room temperature to 120°C at 5°C/min, reaching a plateau at

101 120°C for 1 h and finally returning to room temperature at approx. -5°C/min. The white precipitates were washed

102 by successive centrifugation/redispersion in water. Powders were finally obtained by freeze-drying.

103

104 *2.3 Catalyst characterization techniques*

105 X-ray diffractograms were obtained by a Bruker D8 using Co Kα_1 radiation, λ = 1,789 Å and a scintillation counter.

106 The rutile ratio was calculated according to the law X$_R$= I$_R$(110)/((0.884*I$_A$(101)+ I$_R$(110)) [22], I$_R$(110) being the

107 integrated intensity of rutile (110) peak and I$_A$(101) the integrated intensity of anatase (101) peak, after signal

108 deconvolution. Specific surface area was measured by nitrogen gas adsorption at 77K with an ASAP2000

109 instrument from Micromeritics. Transmission Electron Microscopy (TEM) was performed on a TECNAI 20F.

110

111 *2.4 Photocatalytic experiments*

112 Experiments were conducted in an immersion well, batch operating photoreactor applying a working volume of 500

113 mL. UV irradiation was provided by an 11W low-pressure blacklight fluorescent lamp (PLS G23, Casell Lighting)

114 emitting predominantly at 365 nm. The photon flux emission of the lamp was determined by potassium ferrioxalate

115 actinometer, as described by Murov et al. [23], and found to be 4.98 x 10^{-6} Einstein/s.

116　In a typical run, SAC or BPA solution was loaded in the photoreactor and the appropriate amount of catalyst was

117　added. The slurry solution in the reactor was continuously magnetically stirred to promote uniform dispersion of

118　catalyst powder and dissolved oxygen. At the beginning of each experiment, the solution was stirred in the dark

119　for 30 min to obtain adsorption-desorption equilibrium of organic pollutants onto the catalyst surface. The lamp was

120　then switched on and at regular time intervals, samples were withdrawn and filtered through 0.45 μm syringe filters

121　and further analysed in terms of their organic content. All the experiments were conducted at room temperature

122　(i.e. 22 ^{o}C) and natural pH of SAC and BPA solutions (~ 4.6 and 6.4 for SAC and BPA, respectively). Also, during

123　all experimental runs, the photocatalytic set-up was covered with aluminium foil to prevent irradiation losses and

124　to minimise penetration of ambient light.

125

126　*2.5　Analytical techniques*

127　BPA or SAC concentration in filtrate samples was measured by means of a high performance liquid

128　chromatography (HPLC) system (S200 Pump, S225 Autosampler, Perkin Elmer) coupled with a diode array

129　detector (S200 EP, Perkin Elmer). Samples were separated by reverse phase (RP) chromatography using a C18

130　Luna (Phenomenex) column (5u, 250 x 4.6 mm). HPLC method for SAC was obtained from Trandafil et al. (2009)

131　[24] and was appropriately modified. The mobile phase consisted of 85 vol.% 0.02 M KH_2PO_4 and 15 vol.% CH_3CN

132　fed at a flow rate of 1 mL/min. The elution was isocratic and the injection volume was 40 μL. The detection

133　wavelength was at λ=216 nm. BPA concentration was measured by HPLC method obtained by Daskalaki et al.

134　(2011) [25] at a wavelength of 225 nm. The mobile phase was a mixture of water/acetonitrile (35/65, v/v) at a flow

135　rate of 1 mL/min. The solvents were eluted isocratically and the injection volume was kept at 40 μL.

136　The degree of SAC and BPA photomineralisation was determined by measuring the residual organic concentration

137　by a TOC analyser (Shimadzu TOC-V$_{CPH}$).

138

139　*2.6　Catalyst recovery and reuse*

140　Experiments were carried out to assess the photocatalytic activity of the prepared catalysts after three successive

141　photocatalytic runs. Catalyst recovery was performed at the end of the each cycle, after centrifuging the reactant

142　mixture, to separate catalyst particles from the supernatant effluent. The obtained TiO_2 precipitate was then reused,

143   as the catalyst, for the successive photocatalytic run. The effect of sonication on catalytic performance was also

144   investigated by placing, at the beginning of each cycle, the reactant mixture into an ultrasound bath for 10 min.

145

146   **3   Results and Discussion**

147   *3.1   Catalyst characterization*

148   The specific surface area of the pure anatase (ANA), 15% rutile (R15) and 30% rutile (R30) catalyst samples was

149   197, 201, and 172 m^2/g, respectively, with the corresponding equivalent spherical diameters being 7.8, 7.6, and

150   8.9 nm. These relatively small particle sizes suggest a low particle growth step after nucleation during

151   thermohydrolysis with well-crystallised particles, contrary to other methods requiring calcination. XRD

152   characterizations for the produced TiO_2 nanocomposites are shown in Figure 1, where it is clear that Ti(IV)

153   thermohydrolysis in sulphuric medium yields pure anatase particles. Furthermore, the R15 and R30 samples,

154   mentioned in this Figure, show that the incorporation of a small amount of Sn^{4+} in the crystal lattice is sufficient to

155   induce considerable rutile crystallisation. Indeed, XRD measurements indicate not only remaining anatase

156   crystallisation but also rutile crystallisation revealed by the (110), (101) and (111) peaks' emergence. Moreover,

157   no peak indicating SnO_2 crystallisation is observed, bearing out that Sn^{4+} ions are incorporated into TiO_2 lattice

158   inducing rutile crystallisation.

159

160   Figure 1

161

162   Finally, TEM observations shown in Figure 2 indicate that nanocrystals are much agglomerated and form spherical

163   substructures of around 100 nm size. In addition to the specific surface area values, these observations suggest

164   that the synthesised structures are porous agglomerates. At higher magnification, it can be seen that reticular plans

165   are very oriented between neighbour nanocrystals.

166

167   Figure 2

168

169   *3.2   Evaluation of photocatalytic activity*

170   To evaluate the relative activity of the prepared catalysts ANA, R15 and R30, preliminary experiments were carried

171   out at 5 mg/L SAC or BPA initial concentration and 50 mg/L catalyst loading. In addition, experiments were

172   performed in the presence of P25, KR7050 and PC105 photocatalysts, at the same operating conditions, to

173   establish a comparison against commercially available catalysts. It was observed that the highest SAC and BPA

174   removal (i.e. 98% and 99%, respectively) was obtained when P25 was used as the catalyst. 67% and 38% of SAC

175   and BPA, respectively, was removed in the presence of PC105, whereas KR7050 resulted in 43% degradation of

176   both organics within 90 min of photocatalytic treatment (data not shown). On the other hand, the three prepared

177   catalysts, namely ANA, R15 and R30, yielded similar efficiencies with each other (Figure 3). Specifically, their

178   performance ranged from 21 to 27% and from 22 to 25% in terms of SAC and BPA removal, respectively, indicating

179   that, under these experimental conditions, anatase–rutile interfaces do not affect SAC or BPA degradation.

180   However, as shown in our previous study, where the photocatalytic degradation of phenol in the presence of such

181   catalysts was examined, it was found that anatase–rutile interfaces could affect process efficiency [19]. Specifically,

182   total phenol (with C_0=7.5 mg/L) degradation was achieved in the presence of 400 mg/L of 15% rutile and after

183   about 90 min of treatment, while phenol degradation was about 75% and 80% in the presence of pure anatase

184   and 30% rutile, respectively. Also, Fresno et al. (2009) investigated the gas-phase photocatalytic degradation of

185   trichloroethylene activity in the presence of $Ti_{1-x}Sn_xO_2$ catalysts. They observed a beneficial effect of Sn^{4+} in the

186   activity of TiO_2 which was related to the formation of anatase–rutile mixtures, leading to the highest photocatalytic

187   activity in the sample of composition $Ti_{0.93}Sn_{0.07}O_2$, with anatase:rutile ratio close to 3 [26].

188   Furthermore, experiments were carried out in the dark to assess the adsorption capacity of ANA, R15, R30 and

189   P25 catalysts and results are shown in Figure 3. It was observed that there is no correlation between the adsorption

190   capacity and the corresponding photocatalytic activity, under the experimental conditions applied. For instance,

191   P25, which led to the highest photocatalytic removal of both organics, interestingly yielded very low adsorption

192   capacity (i.e. 3% for BPA and 0.8% for SAC) that was almost the same with that of the ANA, R15, and R30

193   catalysts. Moreover, BPA was found to be adsorbed slightly greater than SAC onto catalyst surface, result that

194   may be ascribed to the different size of the two organics (BPA 228.29 g/mol, SAC 183.18 g/mol), given that all

195   other experimental parameters were identical. It has been previously reported that adsorption of organic

196   substances onto catalytic surface increases with the molecular weight [27], thus explaining the obtained results.

197   Considering the above findings and previously published works, which encourage the use of such type of materials

198   as photocatalysts, we decided to proceed with further experiments, to optimise the process and explore the

199   capacity of these catalysts to eliminate SAC or BPA.

200

201   Figure 3

202

203   *3.3   Effect of the initial solute concentration*

204   Initial SAC or BPA concentration, in the range of 3-10 mg/L, was applied, in the presence of 400 mg/L ANA or R30

205   respectively, to evaluate the effect of initial solute concentration on photocatalytic performance. In Figures 4 and

206   5, it becomes apparent that the increase in the initial organic concentration, at a given catalyst loading, leads to

207   decreased removal efficiency. Specifically, the increase of SAC concentration from 3 to 10 mg/L resulted in the

208   gradual removal decrease from 88% to 52% (Figure 4). Similarly, the BPA conversion rate decreased progressively

209   from 48% to 17% when the initial BPA load increased from 3 to 10 mg/L (Figure 5). In both cases, the results were

210   found to approach well the pseudo-first order reaction model. Plots of the logarithm of normalised SAC and BPA

211   concentration against time resulted in straight lines with the coefficient of linear regression of data fitting, r^2, ranging

212   from 98 to 99% and from 94 to 99% for SAC and BPA, respectively (data not shown). In addition, there is an almost

213   linear relationship between the rate constant, k, and the initial solute concentration as can be seen in the inset

214   graphs of Figures 4 and 5. For example, regarding BPA photocatalytic degradation when its initial concentration is

215   doubled (e.g. from 5 mg/L to 10 mg/L) then the reaction rate constant is decreased by almost two times from

216   0.0049 min^{-1} to 0.0026 min^{-1}. At a fixed catalyst loading, efficiency is dictated by the catalyst active sites to organic

217   molecules ratio. In other words, at relatively low solute loading the active sites provided by the semiconductor are

218   in excess and can uptake most of the organic molecules, thus resulting in higher removal rates. The increase of

219   the initial SAC or BPA concentration results in saturation of the limited catalyst surface by the organic molecules

220   and their reaction by-products that further affects the photonic efficiency and subsequently the degradation rates,

221   thus explaining the above findings [25].

222   Several studies have demonstrated the evolution of toxic intermediates during the photocatalytic treatment of EDCs

223   [12, 28]. Calza et al. (2013) evaluated the ecotoxicity of sucralose solutions treated by heterogeneous

224   photocatalysis [12]. They have observed that toxicity increases during treatment due to the formation of

9

225 intermediate compounds more toxic than sucralose. Similarly, Kondrakov et al. (2004) studied the TiO_2

226 photocatalytic degradation of BPA during which they identified potentially genotoxic by-products [28]. In this

227 direction, SAC and BPA mineralization was monitored, at the best conditions assayed (i.e. C_0=3 mg/L and catalyst

228 concentration=400 mg/L), to get an indication regarding the formation of potentially hazardous by-products. Results

229 showed that, the organic content was decreased by 54 and 43% after 90 min of SAC and BPA photocatalytic

230 treatment, respectively. SAC mineralisation was slightly faster than BPA following the same degradation profile

231 with the parent compounds (i.e. SAC or BPA). Nonetheless, discrepancies between the concentration of TOC and

232 parent compounds were observed. Specifically, SAC degradation was 88% while TOC removal was only 54% after

233 90 min of treatment. Similarly, when BPA degradation was 48%, TOC was removed by 43%. These discrepancies

234 indicate the formation of organic by-products during treatment.

235

236 Figure 4

237

238 Figure 5

239

240 *3.4 Effect of catalyst loading*

241 To investigate the effect of catalyst loading on process efficiency, several TiO_2 concentrations (i.e. 50, 200, 400

242 and 600 mg/L) were examined for the photocatalytic degradation of 5 mg/L SAC or BPA concentration. As seen in

243 Figure 6, although SAC degradation increased considerably with catalyst mass, this was not the case for BPA. In

244 detail, SAC removal was 27%, 59%, 81% and 97% in the presence of 50, 200, 400 and 600 mg/L of ANA catalyst,

245 respectively, and thus process efficiency was increased by about 70% when catalyst concentration was increased

246 from 50 to 600 mg/L (Figure 6a). Furthermore, there is a linear relationship between the rate constant, k, and the

247 catalyst concentration, where the increase of ANA in the range of 50-600 mg/L results in *k* increase from 0.0034

248 to 0.0238 min^{-1} (inset graph of Figure 6a). These results are explained by the fact that at higher amounts of TiO_2

249 (i.e. surface area), the increased number of active sites results in higher photogeneration rate of oxidising species,

250 responsible for the photocatalytic oxidation [16]. Likewise, the same trend was followed during BPA degradation;

251 the increase of R30 from 50 to 400 mg/L led to a 12% increase of process efficiency (Figure 6b). Nonetheless,

252 further increase of R30 from 400 to 600 mg/L did not improve the photocatalytic performance, as can be seen in

253   Figure 6b. This is due to the fact that catalyst loading above a certain point, which seems to be around 400 mg/L

254   for BPA, is associated with screening effects, the excessive TiO_2 particles mask the photosensitive active sites,

255   and the removal efficiency becomes independent of the catalyst mass [16]. The effect of catalyst overloading on

256   BPA photocatalytic treatment can also be seen in the inset graph of Figure 6b, where the rate constant, k, increases

257   linearly from 0.0025 to 0.0049 min^{-1} up to 400 mg/L catalyst concentration. However, k remains almost the same

258   (i.e. 0.0053 min^{-1}) with a further TiO_2 increase to 600 mg/L.

259

260   Figure 6

261

262   *3.5   Effect of catalyst reuse*

263 Catalyst recovery and reuse may be a good practice to reduce the operational cost of photocatalysis and hence to

264 promote its competitiveness among other processes for water and wastewater treatment [29]. Considering this,

265 ANA catalyst was subjected to three successive reuse cycles to determine its effectiveness for SAC treatment and

266 the results are presented in Figure 7. It can be observed that the performance was kept stable during the 1st and

267 2nd cycle with SAC removal being 81% and 84%, respectively. Nonetheless, the catalyst effectiveness dropped to

268 70% at the 3rd cycle. This declined performance can be attributed to catalyst loss during the centrifugation recovery

269 process between reuse cycles. It should be noted that, at the end of the 3rd cycle, the residual catalyst was collected

270 by membrane filtration and its concentration was found about 300 mg/L, instead of 400 mg/L which was the initial

271 catalyst loading at cycle 1. Lower catalyst loading means fewer active sites for the photogeneration of oxidising

272 species and therefore lower solute degradation, thus explaining the above result. Another possible explanation

273 might be the depletion of TiO_2 active sites by residual unreacted SAC molecules, reaction by-products or

274 intermediates and thus less available active sites for photocatalytic oxidation [18, 30, 31]. Nevertheless, loss of

275 catalytic activity does not take place in this case, since the obtained 70%, at cycle 3, is the expected SAC removal

276 percentage in the presence of 300 mg/L ANA, based on results shown in section 3.4, which are also presented in

277 the inset graph of Figure 7. This was expected since, the initial SAC concentration of 5 mg/L is a low adsorbate

278 concentration that cannot significantly affect the formation of free radicals and other reactive oxidative species

279 (ROS) on catalyst surface [32]. Moreover, Fernández-Ibáñez et al. (2003) have used a similar methodology for

280 catalyst recovery and they reported that there is no TiO2 deactivation, when TiO2 reuse follows its separation from

281 the reactant solution [33].

282 Furthermore, additional catalyst reuse experiments were performed with the catalyst being subjected to ultrasound

283 cleaning (US) before its further use, in order to determine the impact of US on catalyst activity (Figure 7). It is well-

284 known that US can remove impurities from the surface of heterogeneous metal catalysts, such as TiO_2, and can

285 bring the reactant materials into more intimate contact with the catalyst surface, thus resulting in increased reaction

286   rates. Also, US assists catalyst dispersion and emulsification and can, therefore, increase the available contact

287   surface area, which enhances chemical reactions between the components of the emulsion [34]. In this case, it is

288   clear in Figure 7 that US did not improve the process efficiency. SAC removal remained unchanged at 81% and

289   84% during the 1st and 2nd reuse cycles, respectively, while the removal at the 3rd cycle was decreased about 4%

290   compared to the respective experiments in the absence of US. This indicates that photocatalytic degradation

291   mainly takes place through free radical and other reactive oxidative species (ROS) reactions and that catalyst

292   agglomeration, as well as the presence of unreacted SAC molecules and by-products on the catalyst surface, was

293   not a limiting factor in the system under study. Also, the negligible effect of US can be attributed to catalyst loss,

294   which was greater than in the absence of US, between reuse cycles. After the end of the 3rd reuse cycle, the

295   residual catalyst concentration was estimated at about 200 mg/L (i.e. 100 mg/L less than the residual catalyst in

296   the corresponding experiment without US; the degree of agglomeration may be reduced by fracture in an ultrasonic

297   field [34] and thus higher amounts of catalyst are lost through centrifugation and membrane filtration).

298

299   Figure 7

300

301   **4   Conclusions**

302   The photocatalytic treatment of saccharin (SAC), an emerging persistent contaminant, and bisphenol-A (BPA), a

303   well-known endocrine disruptor, was studied. In this direction, interfaced anatase–rutile photocatalysts were

304   produced by thermohydrolysis in the presence of small amounts (< 1%) of Sn(IV), which act as a rutile phase

305   promoter. The activity of these catalysts was evaluated in terms of SAC and BPA degradation. Furthermore, the

306   effect of operating conditions, such as initial solute concentration, catalyst type, loading and reuse, on

307   photocatalytic performance was assessed and the conclusions drawn are summarised as follows:

308   -   The photocatalytic efficiency of all novel TiO_2 nanocomposites was very similar in terms of SAC or BPA

309   degradation. Factors that affected mostly the process performance were the initial organics concentration

310   and the catalyst loading. Reaction rate constants increased when the initial solute concentration was

311   decreased and when catalyst concentration was increased up to 400 mg/L. A further increase to 600 mg/L

312   did not improve BPA degradation due to masking effects ascribed to excessive catalyst particles. TOC

313   measurements revealed the presence of transformation products after the end of treatment, thus

314   indicating the need for eco-toxicity estimation before any further scaling-up of the process.

315   -   The recycled catalyst was used in three successive cycles without losing much of its efficiency and thus

316   yielded 70% SAC removal at the end of the 3rd cycle. Finally, ultrasound cleaning of the reactant mixture,

317   at the beginning of each reuse cycle, was applied, in additional experimental runs, and was revealed to

318   have no effect on treatment efficiency.

319

320 **References**

321 [1] Z.-h. Liu, Y. Kanjo, S. Mizutani, Removal mechanisms for endocrine disrupting compounds (EDCs) in

322 wastewater treatment — physical means, biodegradation, and chemical advanced oxidation: A review, Science

323 of The Total Environment, 407 (2009) 731-748.

324 [2] V. Koutantou, M. Kostadima, E. Chatzisymeon, Z. Frontistis, V. Binas, D. Venieri, D. Mantzavinos, Solar

325 photocatalytic decomposition of estrogens over immobilized zinc oxide, Catalysis Today, 209 (2013) 66-73.

326 [3] Z. Sang, Y. Jiang, Y.-K. Tsoi, K.S.-Y. Leung, Evaluating the environmental impact of artificial sweeteners: A

327 study of their distributions, photodegradation and toxicities, Water Research, 52 (2014) 260-274.

328 [4] J. Tijani, O. Fatoba, L.F. Petrik, A Review of Pharmaceuticals and Endocrine-Disrupting Compounds:

329 Sources, Effects, Removal, and Detections, Water Air Soil Pollut, 224 (2013) 1-29.

330 [5] J.-C. Sin, S.-M. Lam, A.R. Mohamed, K.-T. Lee, Degrading Endocrine Disrupting Chemicals from Wastewater

331 by TiO2 Photocatalysis: A Review, International Journal of Photoenergy, 2012 (2012).

332 [6] M.R. Weihrauch, V. Diehl, Artificial sweeteners—do they bear a carcinogenic risk?, Annals of Oncology, 15

333 (2004) 1460-1465.

334 [7] A. Zygler, A. Wasik, J. Namieśnik, Analytical methodologies for determination of artificial sweeteners in

335 foodstuffs, TrAC Trends in Analytical Chemistry, 28 (2009) 1082-1102.

336 [8] M. Scheurer, H.-J. Brauch, F.T. Lange, Analysis and occurrence of seven artificial sweeteners in German

337 waste water and surface water and in soil aquifer treatment (SAT), Analytical and Bioanalytical Chemistry, 394

338 (2009) 1585-1594.

14

339 [9] F.T. Lange, M. Scheurer, H.-J. Brauch, Artificial sweeteners—a recently recognized class of emerging

340 environmental contaminants: a review, Analytical and Bioanalytical Chemistry, 403 (2012) 2503-2518.

341 [10] D.R. Van Stempvoort, J.W. Roy, S.J. Brown, G. Bickerton, Artificial sweeteners as potential tracers in

342 groundwater in urban environments, Journal of Hydrology, 401 (2011) 126-133.

343 [11] M. Scheurer, F.R. Storck, H.-J. Brauch, F.T. Lange, Performance of conventional multi-barrier drinking water

344 treatment plants for the removal of four artificial sweeteners, Water Research, 44 (2010) 3573-3584.

345 [12] P. Calza, V.A. Sakkas, C. Medana, A.D. Vlachou, F. Dal Bello, T.A. Albanis, Chemometric assessment and

346 investigation of mechanism involved in photo-Fenton and TiO2 photocatalytic degradation of the artificial

347 sweetener sucralose in aqueous media, Applied Catalysis B: Environmental, 129 (2013) 71-79.

348 [13] A.J. Li, O.J. Schmitz, S. Stephan, C. Lenzen, P.Y.-K. Yue, K. Li, H. Li, K.S.-Y. Leung, Photocatalytic

349 transformation of acesulfame: Transformation products identification and embryotoxicity study, Water Research,

350 89 (2016) 68-75.

351 [14] S. Malato, P. Fernández-Ibáñez, M.I. Maldonado, J. Blanco, W. Gernjak, Decontamination and disinfection

352 of water by solar photocatalysis: Recent overview and trends, Catalysis Today, 147 (2009) 1-59.

353 [15] Y. Zhang, J.L. Zhou, Occurrence and removal of endocrine disrupting chemicals in wastewater,

354 Chemosphere, 73 (2008) 848-853.

355 [16] J.-M. Herrmann, Heterogeneous photocatalysis: fundamentals and applications to the removal of various

356 types of aqueous pollutants, Catalysis Today, 53 (1999) 115-129.

357   [17] N.P. Xekoukoulotakis, C. Drosou, C. Brebou, E. Chatzisymeon, E. Hapeshi, D. Fatta-Kassinos, D.

358   Mantzavinos, Kinetics of UV-A/TiO2 photocatalytic degradation and mineralization of the antibiotic

359   sulfamethoxazole in aqueous matrices, Catalysis Today, 161 (2011) 163-168.

360   [18] E. Chatzisymeon, E. Stypas, S. Bousios, N.P. Xekoukoulotakis, D. Mantzavinos, Photocatalytic treatment of

361   black table olive processing wastewater, Journal of Hazardous Materials, 154 (2008) 1090-1097.

362   [19] A. Pichavant, E. Provost, M.-H. Berger, W. Fürst, J.-F. Hochepied, Interfaced titanium dioxide anatase–rutile

363   nanocomposites by thermohydrolysis in presence of small amounts of Sn(IV) and their photocatalytic properties,

364   Colloids and Surfaces A: Physicochemical and Engineering Aspects, 462 (2014) 64-68.

365   [20] G. F. Ferreira, M. G. Maniero, J. R. Guimarães, Degradation of Sucralose by Peroxidation Assisted with

366   Ultraviolet Radiation and Photo-Fenton, International Journal of Engineering and Technology, 7 (2015) 438-444.

367   [21] S.W. Chen, W.C. Li, Z.G. Sun, H.Y. Xie, Degradation of Artificial Sweetener Saccharin Sodium by Advanced

368   Oxidation Technology, Applied Mechanics and Materials, 448-453 (2014) 7-10.

369   [22] A.A. Gribb, J.F. Banfield, Particle size effects on transformation kinetics and phase stability in

370   nanocrystalline TiO2, American Mineralogist, 82 (1997) 717-728.

371   [23] S.L. Murov, I. Carmichael, G.L. Hug, Handbook of Photochemistry, Second Edition, Taylor & Francis1993.

372   [24] I. Trandafir, V. Nour, M.E. Ionică, Development and validation of an HPLC methods for simulatneous

373   quantification of acesulfame-K, saccharin, aspartame, caffeine and benzoic acid in cola soft drinks, Scientific

374   Study & Research X(2009) 185-194.

375   [25] V.M. Daskalaki, Z. Frontistis, D. Mantzavinos, A. Katsaounis, Solar light-induced degradation of bisphenol-A

376   with TiO2 immobilized on Ti, Catalysis Today, 161 (2011) 110-114.

377   [26] F. Fresno, D. Tudela, J.M. Coronado, J. Soria, Synthesis of Ti1−xSnxO2 nanosized photocatalysts in

378   reverse microemulsions, Catalysis Today, 143 (2009) 230-236.

379   [27] A.R. Khataee, M.N. Pons, O. Zahraa, Photocatalytic degradation of three azo dyes using immobilized TiO2

380   nanoparticles on glass plates activated by UV light irradiation: Influence of dye molecular structure, Journal of

381   Hazardous Materials, 168 (2009) 451-457.

382   [28] A.O. Kondrakov, A.N. Ignatev, F.H. Frimmel, S. Bräse, H. Horn, A.I. Revelsky, Formation of genotoxic

383   quinones during bisphenol A degradation by TiO2 photocatalysis and UV photolysis: A comparative study,

384   Applied Catalysis B: Environmental, 160–161 (2014) 106-114.

385   [29] N. Miranda-García, S. Suárez, M.I. Maldonado, S. Malato, B. Sánchez, Regeneration approaches for TiO2

386   immobilized photocatalyst used in the elimination of emerging contaminants in water, Catalysis Today, 230

387   (2014) 27-34.

388   [30] M. Argyle, C. Bartholomew, Heterogeneous Catalyst Deactivation and Regeneration: A Review, Catalysts, 5

389   (2015) 145.

390   [31] S. Salaeh, M. Kovacic, D. Kosir, H. Kusic, U. Lavrencic Stangar, D.D. Dionysiou, A. Loncaric Bozic, Reuse

391   of TiO2-based catalyst for solar driven water treatment; thermal and chemical reactivation, Journal of

392   Photochemistry and Photobiology A: Chemistry, 333 (2017) 117-129.

393   [32] J. Araña, E. Tello Rendón, J.M. Doña Rodríguez, J.A. Herrera Melián, O. González Díaz, J. Pérez Peña,

394   High concentrated phenol and 1,2-propylene glycol water solutions treatment by photocatalysis: Catalyst

395   recovery and re-use, Applied Catalysis B: Environmental, 30 (2001) 1-10.

396   [33] P. Fernández-Ibáñez, J. Blanco, S. Malato, F.J.d.l. Nieves, Application of the colloidal stability of TiO2

397   particles for recovery and reuse in solar photocatalysis, Water Research, 37 (2003) 3180-3188.

398   [34] D. Ensminger, Ultrasonics: Fundamentals, Technology, Applications, Second Edition, Revised and
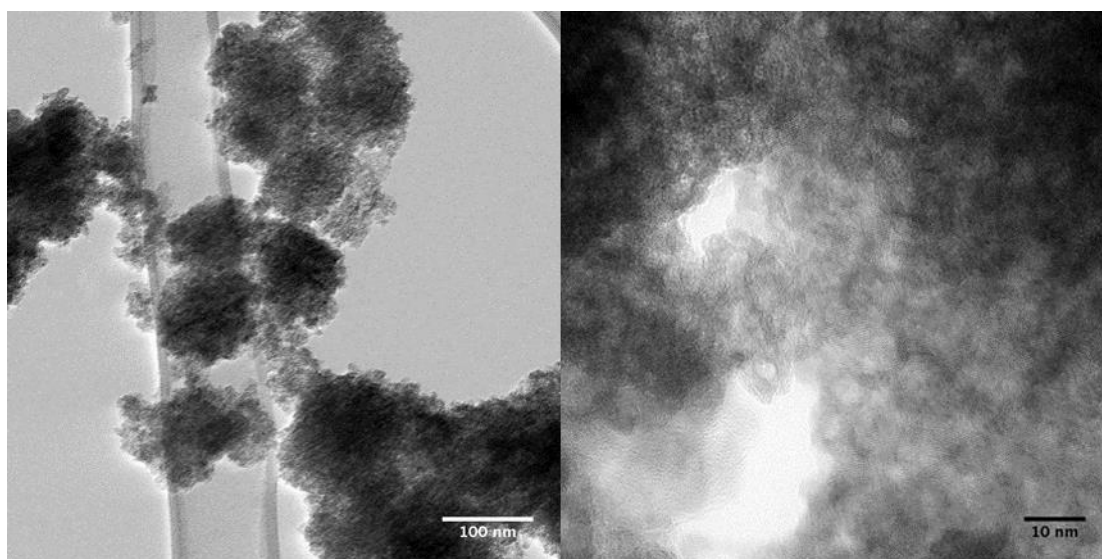
399   Expanded, 1988.
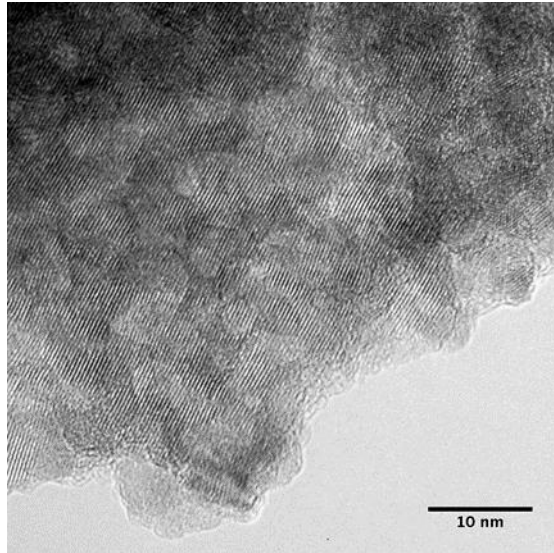
400

401

402

List of Figures
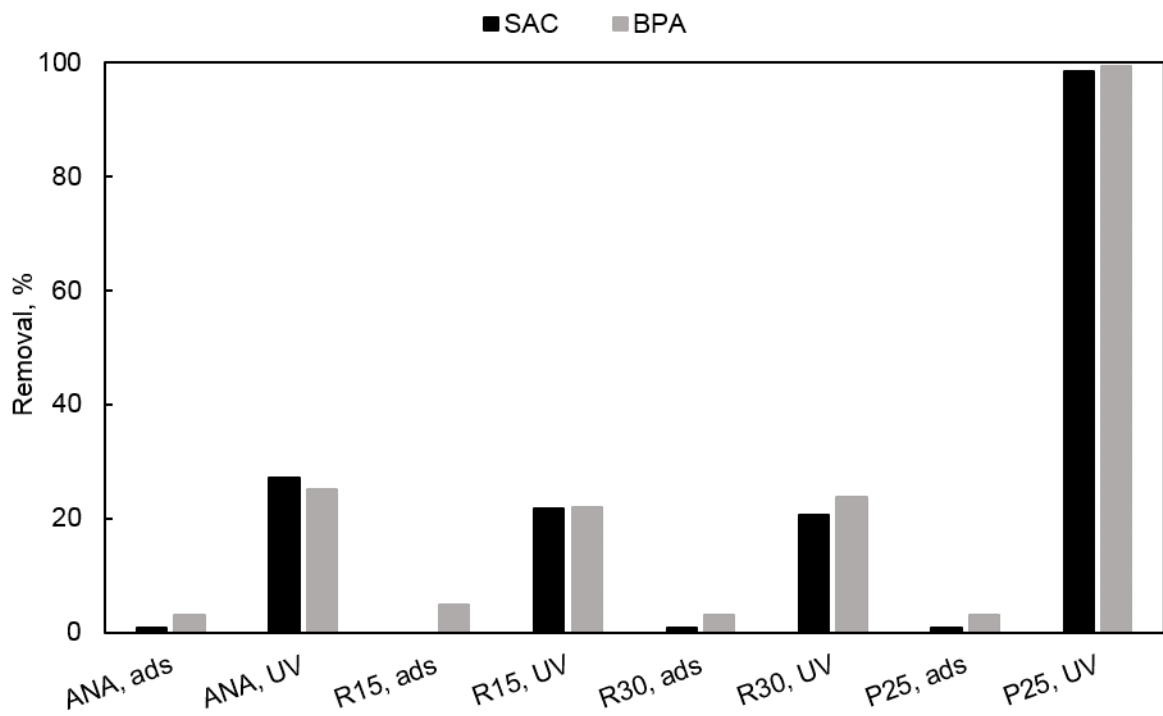
420

421

422 Figure 1
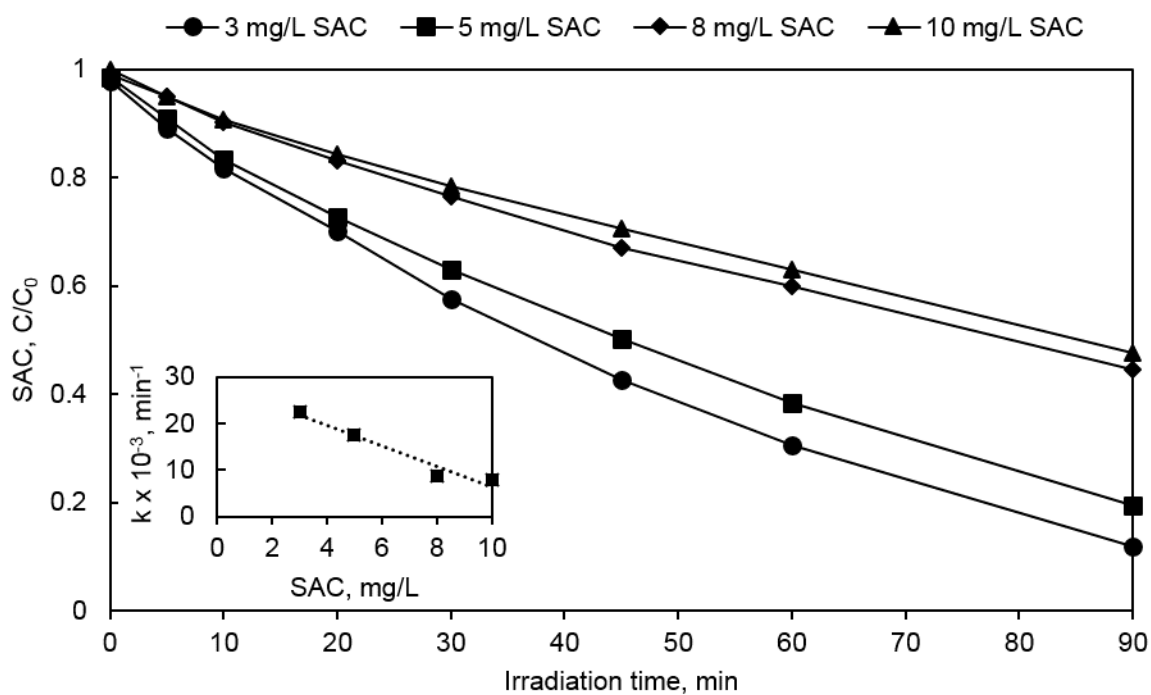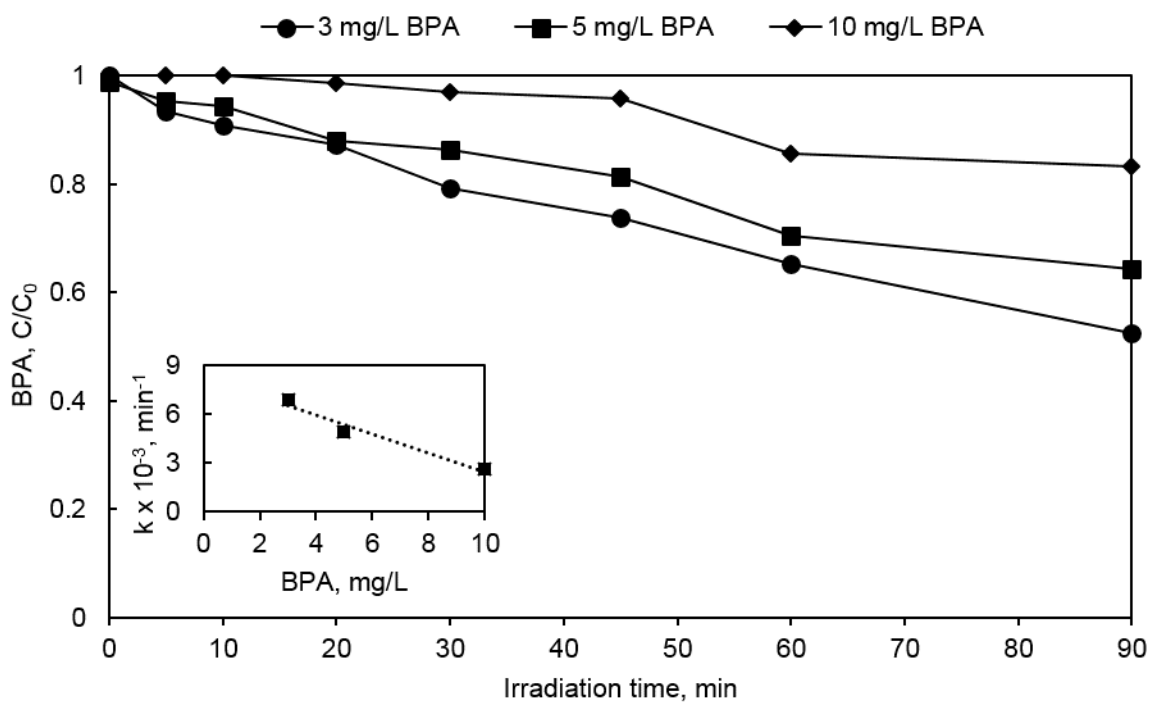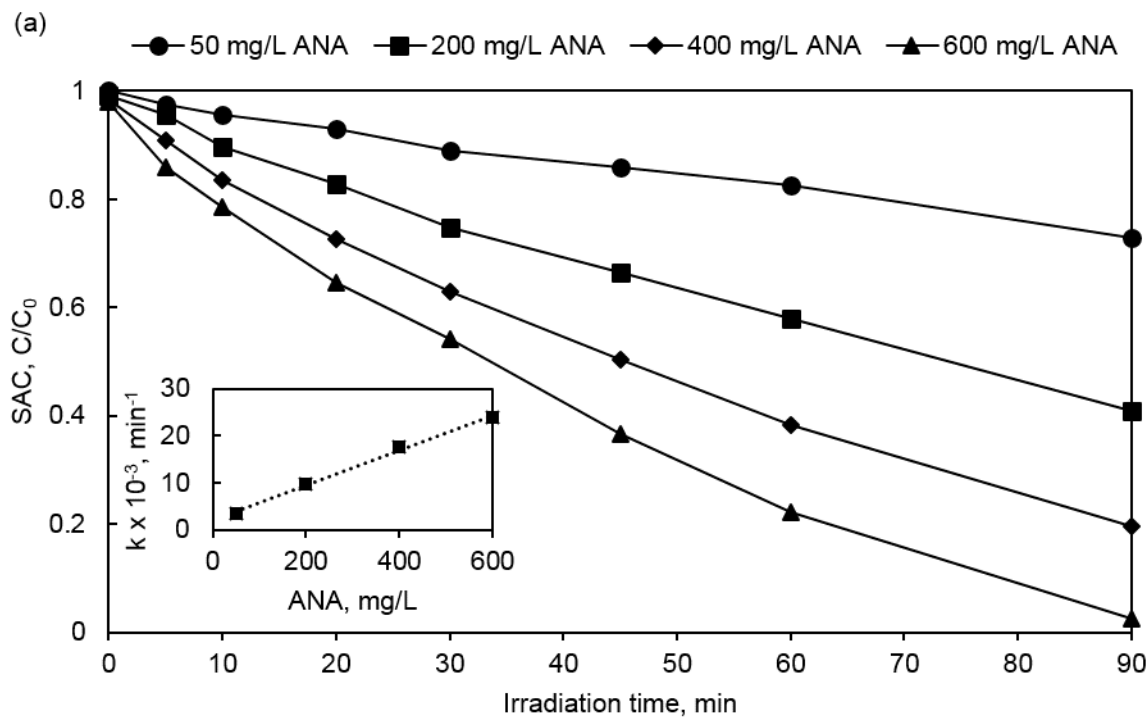
423

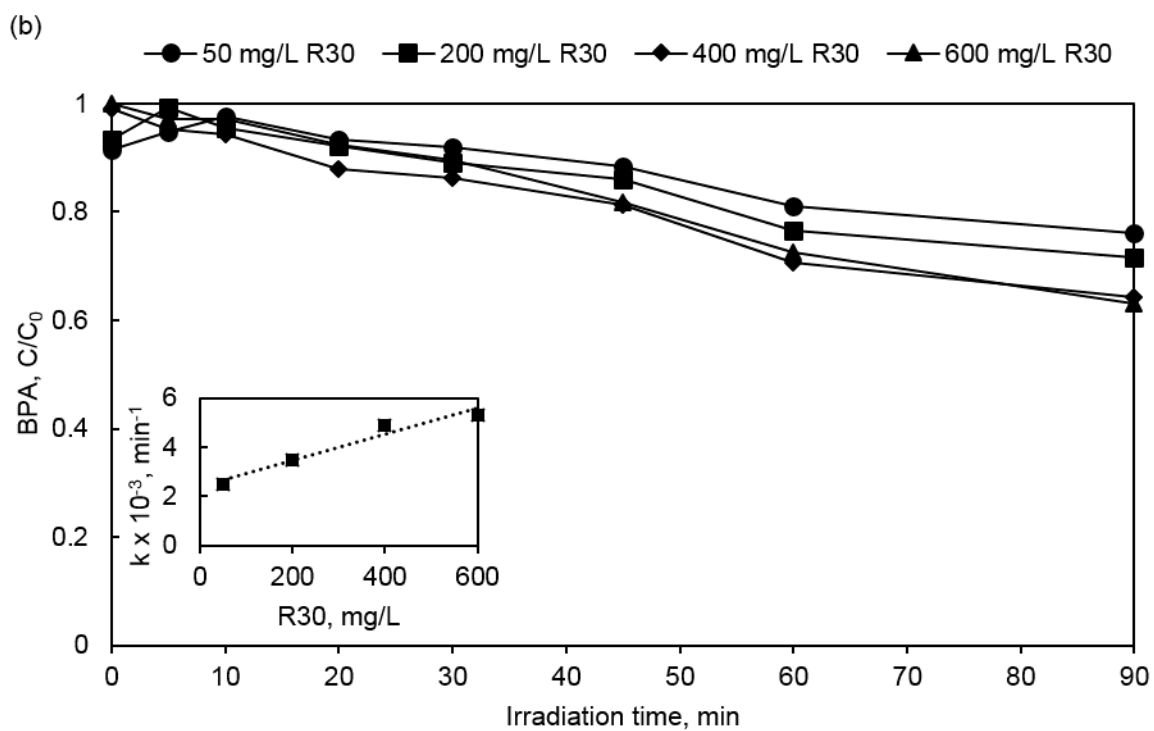424

425

426   Figure 2

427

428

429   Figure 3
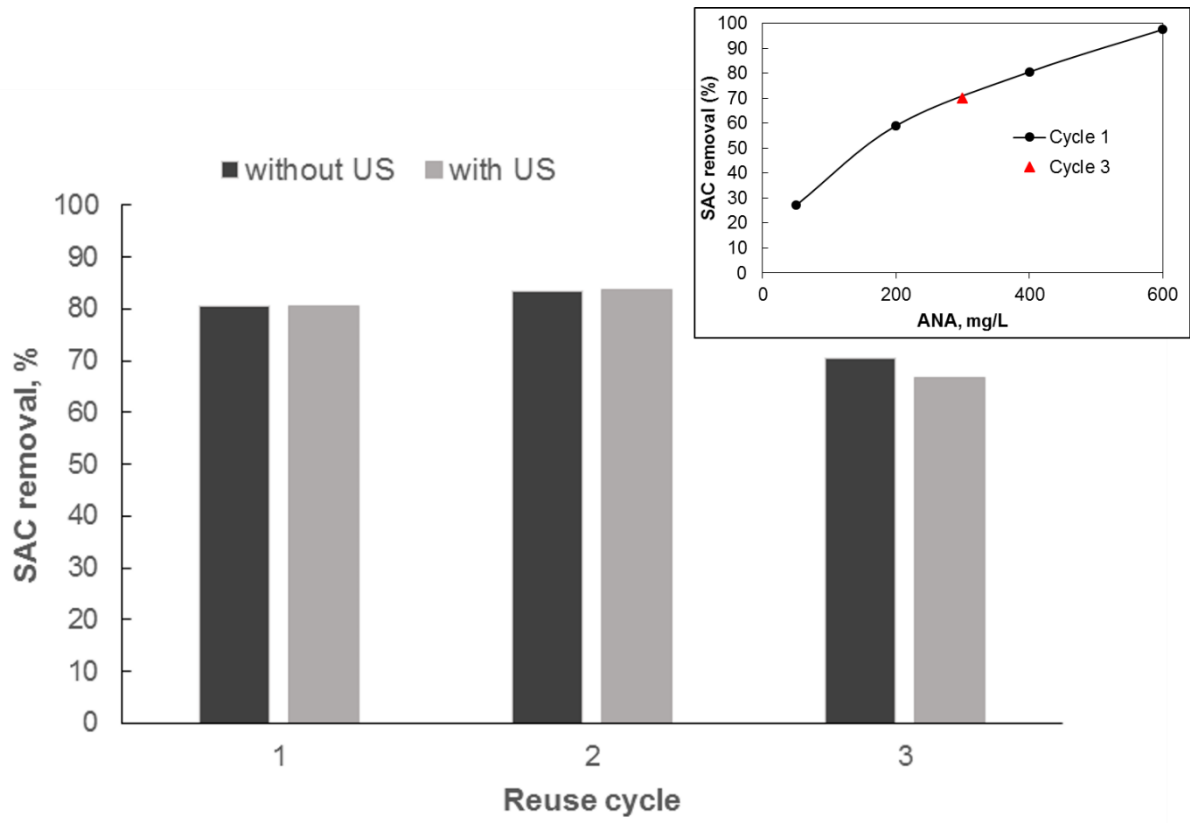
430

431

432   Figure 4

433

434   Figure 5

(a)

— 50 mg/L ANA — 200 mg/L ANA — 400 mg/L ANA — 600 mg/L ANA

435

(b)

— 50 mg/L R30 — 200 mg/L R30 — 400 mg/L R30 — 600 mg/L R30

436

437   Figure 6

438

439   Figure 7

440

441

442